Inter- and intra-event rainfall partitioning dynamics of two typical xerophytic shrubs in the Loess Plateau of China

Jinxia An[1,2], Guangyao Gao[1,2,5], Chuan Yuan[3], Juan Pinos[4], Bojie Fu[1,2,5]

5

[1]State Key Laboratory of Urban and Regional Ecology, Research Center for Eco-Environmental Sciences, Chinese Academy of Sciences, Beijing 100085, China

[2]University of Chinese Academy of Sciences, Beijing 100049, China

[3]State Key Laboratory of Subtropical Silviculture, Zhejiang A&F University, Hangzhou
10 311300, China

[4]Surface Hydrology and Erosion Group, Institute of Environmental Assessment and Water Research (IDAEA-CSIC), Barcelona 08034, Spain

[5]National Observation and Research Station of Earth Critical Zone on the Loess Plateau in Shaanxi, Xi'an 710061, China

15

Correspondence to: Guangyao Gao (gygao@rcees.ac.cn)

Abstract. Rainfall is known as the main water replenishment in dryland ecosystem, and rainfall partitioning by vegetation reshapes the spatial and temporal distribution patterns of
20 rainwater entry into the soil. The dynamics of rainfall partitioning have been extensively studied at the inter-event scale, yet very few studies have explored its finer intra-event dynamics and the relating driving factors for shrubs. Here, we conducted a concurrent in-depth investigation of all rainfall partitioning components at inter- and intra-event scales for two typical xerophytic shrubs (*Caragana korshinskii* and *Salix psammophila*) in the

25   Liudaogou catchment of the Loess Plateau, China. The event throughfall (TF), stemflow (SF), and interception loss (IC) and their temporal variations within the rainfall event as well as the meteorological factors and vegetation characteristics were systematically measured during the 2014-2015 rainy seasons. Our results showed that *C. korshinskii* had significantly higher SF percentage (9.2%) and lower IC percentage (21.4%) compared to *S. psammophila* (3.8%

30   and 29.5%, respectively), but their TF percentages were not significantly different (69.4% vs. 66.7%). At the intra-event scale, TF and SF of *S. psammophila* was initiated (0.1 vs. 0.3 h and 0.7 vs. 0.8 h) and peaked (1.8 vs. 2.0 h and 2.1 vs. 2.2 h) more quickly, and TF of *S. psammophila* lasted longer (5.2 vs. 4.8 h), delivered more intensely (4.3 vs. 3.8 mm·h^{-1}), whereas SF of *C. korshinskii* lasted longer (4.6 vs. 4.1 h), delivered more intensely (753.8 vs.

35   471.2 mm·h^{-1}). For both shrubs, rainfall amount was the most significant factor influencing inter-event rainfall partitioning, and rainfall intensity and duration controlled the intra-event TF and SF variables. The *C. korshinskii* with larger branch angle, more small branches and smaller canopy area, has an advantage to produce stemflow more efficiently over *S. psammophila*. The *S. psammophila* has lower canopy water storage capacity to generate and

40   peak throughfall and stemflow earlier, and it has larger aboveground biomass and total canopy water storage of individual plant to produce higher interception loss compared to *C. korshinskii*. These findings contribute to the fine characterization of shrub-dominated eco-hydrological processes, and improve the accuracy of water balance estimation in dryland ecosystem.

45

1 Introduction

Rainfall is known as the main replenishment of water resources in arid and semi-arid areas, and water resource is the key factor limiting the function of arid ecosystems (Chesson et al., 2004; Cayuela et al., 2018; Magliano et al., 2019a). Before entering into soil, rainfall is redistributed by plant canopies into throughfall (TF, diffuse water input), stemflow (SF, point water input), and interception loss (IC, evaporation). The sum of TF and SF is defined as "net rainfall". Differences in the distribution of net rainfall caused by plant canopy interception alter the spatial and temporal patterns of rainfall entry into the soil (Martinez-Meza and Whitford, 1996; Li et al., 2009; Van Stan II et al., 2020), and further profoundly affect the water use efficiency of vegetation and ecosystem sustainability (Xu and Li, 2006; Lacombe et al., 2018; Molina et al., 2019). In addition, net rainfall could regulate vegetation physiological metabolic processes through nutrient enrichment (Levia and Frost, 2003; Zhang et al., 2016; Van Stan II et al., 2017; Tonello et al., 2021), ultimately affecting the carbon balance of ecosystems (Chu et al., 2018; Jia et al., 2016). In light of the important role of rainfall partitioning in regulating soil moisture and vegetation patch pattern, investigations of the rainfall partitioning dynamics are imperative for a better understanding of the soil-water-vegetation relationships (Molina et al., 2019; Van Stan II et al., 2020; Zhang et al., 2021a).

Studies on rainfall partitioning have been broadly carried out in different climatic zones and various types of vegetation (Gordon et al. 2020; Rivera and Van Stan II, 2020; Zhang et al., 2021b; Yue et al., 2021). Based on a comprehensive global synthesis, Yue et al. (2021)

found that most TF and SF observations were measured in forests ($n = 718$ and $n = 816$, respectively), and that in shrublands was scarce ($n = 43$ and $n = 63$, respectively), which was mainly due to that the shrubs have multiple branches and the rainfall partitioning of shrubs is

70   difficult to be measured compared to forests. Shrubs are the dominant vegetation type in drylands, forming fertile islands by intercepting water and trapping sediments, thus providing important ecosystem goods and services (Levia and Frost, 2003; Llorens and Domingo, 2007; Soulsby et al., 2017). However, the lack of information on the detailed dynamics of rainfall partitioning processes induced by shrubs due to limited studies hinders us form a clear

75   understanding of shrubs' eco-hydrological role in shaping and sustaining drylands.

Most of the existing studies on the rainfall partitioning by shrub are based on the inter-event scale (Garcia-Estringana et al., 2010; Magliano et al., 2019a). Magliano et al. (2019a) synthesized that for 27 shrub species in drylands, the mean event-based SF%, TF%, and IC% were 9.4%, 63.0% and 27.6%, respectively. Rainfall partitioning by shrubs has been

80   reported to be determined by biotic and abiotic factors, such as rainfall characteristics (Levia and Frost, 2003; Magliano et al., 2019b) and canopy structure characteristics (Martinez-Meza and Whitford, 1996; Garcia-Estringana et al., 2010; Yue et al., 2021). Take the later for example, vegetation with smooth barks, more branches and vertical branching had advantages on SF generation (Honda et al., 2015; Magliano et al., 2019a; Whitworth-Hulse et

85   al., 2020b), and a simple vegetation structure and low canopy density are generally corresponding to a relatively high TF rate and low IC rate (Soulsby et al., 2017; Yue et al., 2021). The complexity of shrub structure poses challenges to understand the causes of rainfall

partitioning dynamics under different meteorological conditions, and it is necessary to

substantially explore the differences of rainfall partitioning dynamics and main influencing

90   factors among different shrub species (Levia et al., 2010; Sadeghi et al., 2020).

In addition to the inter-event studies, a few intra-event scale studies have also been

reported, which is essential for better understanding of soil moisture distribution and the

hydrological cycle in arid regions (Levia et al., 2010; Levia and Germer, 2015; Cayuela et al.,

2018; Zhang et al., 2021a). For instance, Zhang et al. (2018) investigated the spatial-temporal

95   pattern of TF of *C. korshinskii* in arid area of northern China at high temporal resolution

(10-min intervals), and they found that temporal heterogeneity of rainfall clearly affected the

spatiotemporal dynamics of TF beneath shrub canopies and the wind directions were the main

factor affecting TF in different radial directions. Yuan et al. (2019) described the branch SF

variability of *C. korshinskii* and *S. psammophil*, and they showed that intra-event branch SF

100   variability of xerophytic shrubs temporally depended on rainfall characteristics, with longer

lag times and greater rainfall amount required to initiate branch SF for *C. korshinskii*

compared to *S. psammophila*. It can be found that those studies on temporal dynamics of

shrub rainfall partitioning only explored the single-element process (i.e., throughfall or

stemflow), and ignored interception loss. Concurrent investigation on all rainfall partitioning

105   components and the associated influencing factors at the intra-event scale has rarely been

reported. Furthermore, to the best of author's knowledge, no previous studies have been

reported so far that simultaneously analyzed TF, SF and IC on an intra-event scale in any

shrub species. Therefore, a detailed understanding of shrub rainfall partitioning dynamics at

the intra-event scale with high resolution data is sorely needed to improve mechanistic

110   understanding of shrubs' eco-hydrological role in shaping and sustaining drylands.

This study was designed at the event and process scales to investigate inter-event and

intra-event rainfall partitioning variability, based on field measurements on two dominant

xerophytic shrubs (*C. korshinskii* and *S. psammophila*) during the rainy seasons of 2014-2015

in the Loess Plateau of China. This study integrated the inter-event and intra-event dynamics

115   of rainfall partitioning by combining TF, SF and IC at the individual plant scale. We mainly

seek to (a) compare the dynamic processes of rainfall partitioning between the two shrubs at

both inter-event and intra-event scales, and (b) elucidate the effects of rainfall characteristics

and vegetation structure characteristics on rainfall partitioning at both scales. Such an

improvement in our understanding of the fine-scale mechanism of rainfall partitioning would

120   offer valuable insights regarding shrub-water interactions.

2   Materials and methods

2.1 Site description and experimental design

This study was carried out in the Liudaogou catchment (110°21′-110°23′ E, 38°46′-38°5′ N)

in Shenmu county, Shaanxi Province of China (Fig. 1a). The Liudaogou catchment (6.9 km^2,

125   altitude from 1094 to 1273 m) is located between the northern Loess Plateau and the south

fringe of Mu Us sandy land in North China. This region is characterized by a moderate

temperate continental climate with well-defined rainy and dry seasons. The mean annual

rainfall is 437 mm ranging between 109-891 mm (1971-2013), and the potential evaporation

is 1337 mm yr^{-1} (Jia et al., 2013). Approximately 70-80% of the rainfall events are

130   concentrated in the warm months between July and September and most of them occur in the

form of torrential rain (Yang et al., 2019). The Liudaogou catchment was characterized by the

natural arid scrub steppe before it was artificially vegetated in the past 20 or 30 years for soil

and water conservation, windbreak and sand fixation. The main land use types include

artificial grassland, artificial shrub and farmland, and the main vegetation species are *Stipa*

135   *bungeana*, *C. korshinskii* and *S. psammophila*, which are widely distributed in the arid and

semiarid areas of northwestern China (Yuan et al., 2019). The shrub is distributed sparsely

with distinct interspaces. The actual ground cover fraction covered by shrub canopies was less

than 20%, with the rest of soil being directly exposed to rainfall.

Two representative xerophytic shrubs, *C. korshinskii* and *S. psammophil*a with 20 years

140   old, were used for the study. Both species are multiple-stemmed deciduous perennial shrubs

with inverted cone crowns and without trunks. They have minimal nutrient requirements,

extensive adaptability and strong stress resistance, which makes them superior in adapting to

resource-poor environments. According to the documentation of *Flora of China* (Chao and

Gong, 1999; Liu et al., 2010) and field observations, the *S. psammophila* has an odd number

145   of strip-shaped leaves with 2-4 mm in width and 40-80 mm in length, and the *C. korshinskii*

has pinnate compound leaves arranged opposite or sub-opposite with 6-10 cm in length, and

each pinna has 5 to 8 pairs of ovate leaflets (7-8 mm in length and 2-5 mm in width). We

established two plots (one for *C. korshinskii* and the other for *S. psammophila*) at the

southwestern catchment for field observation (Fig. 1a). The two plots share similar stand

150   conditions, with the sizes of 3294 m^2 and 4056 m^2, elevations of 1179 m and 1207 m, and

slopes of 13° and 18°, respectively. The distance between the two plots do not exceed 1.5 km.

2.2 Field measurements

2.2.1 Measurements of rainfall and meteorological factors

This study focused on the individual shrub rainfall partitioning of *C. korshinskii* and *S.*

psammophila during the 2014-2015 rainy seasons. Gross rainfall was measured using one

tipping-bucket rain gauge with a 0.2 mm resolution (TBRG, with 186.3 cm^2 collection area)

(Onset® RG3-M, Onset Computer Corp., USA) in an open area (Fig. 1b). The rainfall

characteristics, e.g., rainfall amount (RA, mm), rainfall duration (RD, h), rainfall interval (RI,

h), average rainfall intensity (I, mm·h^{-1}), rainfall intensity at 10-min interval (i.e., 0-10 min,

10-20 min,….) since the start of rainfall (I$_{10}$, mm·h^{-1}) were calculated accordingly. For I$_{10}$, the

one after the onset of rainfall is defined as I$_{10\_b}$ (mm·h^{-1}), i.e., the rainfall intensity in the first

10 min. The maximum I$_{10}$ during the rainfall process is defined as I$_{10\_max}$ (mm·h^{-1}). As the

TBRG has a resolution of 0.2 mm, we define a single rainfall event as one that is greater than

0.2 mm and not raining for at least 4 hours apart (Iida et al., 2012). A meteorological station

was set up at the experimental plot to record wind speed (WS, m·s^{-1}) and wind direction (WD,

$^{\circ}$) (Model 03002, R. M. Young Company, Traverse City, Michigan, USA), air temperature (T,

$^{\circ}$C) and relative humidity (H, %) (Model HMP 155, Vaisala, Helsinki, Finland). Data were

measured every 30 s and averaged at 10 min interval by the data logger (Model CR1000,

Campbell Scientific, Inc., USA).

2.2.2 Measurements of vegetation characteristics

Three representative shrub plants with similar crown heights and crown areas were selected

in each shrub species (Table 1). Based on plot investigation, the vegetation traits at the scale of single plant and branch were measured. For each plant, we measured shrub height (SH, m) with a graduated telescopic stick, counted the number of branches (NB), and calculated the projected canopy area (CA, m^2) by measuring canopy diameter following the south-north and east-west direction. The total number of branches was 143 and 218 for selected *C. korshinskii* and *S. psammophila* plants, respectively. For each branch, we measured branch length (BL, cm) with a measuring tape, branch angle (BA, $^\circ$) with a pocket geologic compass, and branch diameter (BD, mm) with a vernier caliper to calculate the total basal area of the shrub (TBA, m^2). Thus, four BD categories (0-10, 10-15, 15-20 and > 20 mm) were defined to ensure the appropriate branch amounts within each category. The measured vegetation traits of *C. korshinskii* and *S. psammophila* plants are shown in Table 1.

Water storage capacity of the canopy is a key factor in determining the amount of interception loss (Levia and Herwitz, 2005; Garcia-Estringana et al., 2010) and SF yield (Van Stan II et al., 2020). We selected 10 representative branches for each shrub species outside the stands, to determine the canopy water storage capacity (C, mL/g) using water immersion method, which was widely used in previous studies (Garcia-Estringana et al., 2010; Wang et al., 2012). The C was calculated as the difference between saturated weight and fresh weight divided by the dry biomass of the selected branch. The *C. korshinskii* and *S. psammophila* had a C of 0.85 mL/g and 0.38 mL/g, respectively. In addition, we estimated the total dry aboveground biomass of single plant (TB) for each species according to the allometric growth model developed by Yuan et al. (2016 and 2017) in the same study area. The

allometric growth model had very high accuracy with R^2 more than 0.92. The total canopy water storage of single plant (C_m = TB times C) was calculated to represent the amount of rainfall absorbed by the shrub canopy during the rainfall event (Table 1).

2.2.3 Measurements of inter-event rainfall partitioning

Manual rain gauges (314.12 cm^2 collection area) were used to measure event TF at eight radial directions (E, SE, S, SW, W, NW, N, NE) beneath each shrub canopy (Fig. 1b). For *C. korshinskii*, eight TF gauges were placed under each *C. korshinskii* plant with 50 cm distance from the base of stems in the eight directions. For *S. psammophila*, twenty TF gauges were placed under each plant, with twelve of them placed in 50 cm, 100 cm, and 150 cm distances from the base of stems in four directions (E, S, W, and N), and eight of them placed in 75 cm and 125 cm distances in the other four directions (SE, SW, NW, and NE). If the rainfall ended during the daytime, we completed the collection of TF samples within two hours after the end of rainfall. If the rainfall ended at night, we completed the collection of samples as early as possible in the next day to minimize evaporation.

A total of 53 branches of *C. korshinskii* (17, 21, 7, 8 for BD categories of 0-10, 10-15, 15-20 and > 20 mm, respectively) and 98 branches of *S. psammophila* (20, 30, 20 and 28 for BD categories of 0-10, 10-15, 15-20, and > 20 mm, respectively) were used to determine SF yield, which covered different types of branches. Funnels constructing of flexible aluminum foil plates were used to collect SF (Fig. 1b). The funnel was fixed to each branch near the base and sealed with neutral silicone caulk, and a 0.5 cm diameter PVC hose was attached vertically to transport SF from the funnel to a container with a lid (SF gauges) with minimum

travel time.

2.2.4 Measurements of intra-event rainfall partitioning

Among the selected plants, one *C. korshinskii* and one *S. psammophila* plant were selected to record the volume and timing of TF and SF with TBRGs at intra-event scale. A TBRG was installed in each of four radial directions (E, S, W, N) beneath the shrub canopy of each species, to measure the temporal variations of TF within the rainfall event (Fig. 1b). To characterize intra-event SF dynamics, six representative branches of different BD categories were selected for each species, using the following selection criteria: no crossover between the experimental branch and adjacent branches, no inflection point from the tip to the base of the branch, and accessible for easy installation and measurement. These branches were distributed across the four BD categories (0-10, 10-15, 15-20, and > 20 mm, respectively). SF TBRGs were covered with the polyethylene films to prevent the accessing of throughflow and splash (Fig. 1b). Unfortunately, some TBRGs lost a substantial amount of stemflow data and were therefore discarded from the analysis. Four branches were finally identified for each species, located in each of the four BD categories to measure intra-event SF (6.7, 13.5, 18.6, and 22.1 mm for *C. korshinskii* and 7.2, 14.4, 18.2, and 31.3 mm for *S. psammophila*).

2.3 Rainfall partitioning calculations

2.3.1 Inter-event rainfall partitioning calculations

For each individual shrub, we measured TF volume for each TF gauges, averaged them, and then converted the volume into TF depth (TF_d, mm) at each rainfall event. And the percentage of TF (TF%, %) was calculated by dividing TF_d by the RA, and the average TF intensity (TFI,

235   mm·h^{-1}) was calculated by dividing TF$_d$ by the TF duration (TFD, h). The TFD was recorded

by TF TBRGs.

The inter-event SF yield was defined as the total SF volume of a single plant in a rainfall event. The SF volumes measured on the selected branches were averaged to obtain the average volume of SF on the branch scale, which multiply the number of branches to obtain

240   the total SF volume from the plant. The shrub-scale SF equivalent water depth (SF$_d$, mm) and the average SF intensity (SFI, mm·h^{-1}) were calculated. The percentage of SF (SF%, %) was converted by dividing SF$_d$ by the RA. The SF$_d$ and SFI were calculated by the following equations (Hanchi and Rapp, 1997; Levia and Germer, 2015):

$$SF_d = (\overline{SF_b} \times n)/(1000 \times CA) \tag{1}$$

245     $$SFI = (\overline{SF_b} \times n)/(10 \times TBA \times SFD) \tag{2}$$

where $\overline{SF_b}$ (ml) is the average volume of SF on the branch scale, n is the number of branches of individual plant, CA (m^2) is the canopy area of individual plant, TBA (cm^2) is the total basal area of individual plant, and SFD is SF duration (h) recorded by SF TBRGs. The parameters 1000 and 10 are the unit conversion factor.

250   The IC depth (IC$_d$, mm) and percentage of IC (IC%, %) were estimated as:

$$IC_d = RA\text{-}TF_d\text{-}SF_d \tag{3}$$

$$IC\% = 100\%\text{-}TF\%\text{-}SF\% \tag{4}$$

The above inter-event rainfall partitioning variables and their explanations are summarized in Table 2.

2.3.2 Intra-event rainfall partitioning calculations

The TF and SF volume and timing within rainfall event were automatically recorded at dynamic intervals between neighboring TBRG tips (0.2 mm). To better reflect fluctuations in rainfall partitioning components, the intra-event TF and SF data were aggregated every 10 minutes to match with the recording interval of gross rainfall. The four TF depths recorded by TBRGs were averaged to obtain the average TF depth at 10-min interval (TF_{d10}, mm). The TF intensity at 10-min interval (TFI_{10}, mm·h^{-1}) was calculated by dividing the TF_{d10} by the 10 min. Meanwhile, SF depth (SF_{d10}, mm) and SF intensity at 10-min interval (SFI_{10}, mm·h^{-1}) were calculated as:

$$SF_{d10} = \sum_{j=1}^{4} \left(186.3 \times SF_{RG,j} \times n_j\right) \Big/ (100 \times CA) \qquad (5)$$

$$SFI_{10} = \sum_{j=1}^{4} \left(186.3 \times SF_{RG,j} \times n_j\right) \Big/ (TBA \times 1/6) \qquad (6)$$

where $SF_{RG,j}$ (mm) is the SF depth of the selected jth branch category recorded by TBRG at 10-min interval (1/6 h), n_j is the number of branches in the jth category of single plant, 4 is the number of BD category (0-10, 10-15, 15-20, and > 20 mm), and 186.3 (cm^2) is the collection area of TBRG. The product of $SF_{RG,j}$ and 186.3 is the SF volume from the branch. The parameter 100 is the unit conversion factor.

Based on the calculated TFI_{10} and SFI_{10}, the maximum TF and SF intensity at 10-min interval (TFI_{10_max} and SFI_{10_max}, respectively, mm·h^{-1}) of each rainfall event can be determined. The descriptive variables for the intra-event rainfall partitioning also include the lag times of TF or SF corresponding to the rainfall event. Based on the temporal data

13

275 recorded by TBRGs (between neighboring tips), the following variables were calculated:

LG_{TF} and LG_{SF} (h), the time lag of TF and SF generation after the start of rainfall,

respectively; LM_{TF}, LM_{SF} and LM_R (h), the time lag of TFI_{10_max}, SFI_{10_max} and I_{10_max} relative

to the onset of rainfall, respectively; and LE_{TF} and LE_{SF} (h), the time lag of TF and SF ending

after the end of rainfall. The intra-event rainfall partitioning variables and their explanations

280 are summarized in Table 2.

2.4 Statistical analysis

Independent-samples T-tests were used to analyze differences in rainfall partitioning

parameters between *C. korshinskii* and *S. psammophila* at both inter-event and intra-event

scales. To detect the effects of meteorological factors on rainfall partitioning, Pearson

285 correlation analysis was used to test the significance between rainfall partitioning parameters

and meteorological factors at the two scales. The significant correlated factors were

double-checked by partial correlation analysis to determine their individual effects on rainfall

partitioning components. Stepwise regression of these indicators was performed by analytical

tests at the 0.05 level of significance to select the most influential factors on rainfall

290 partitioning variables at inter-event and intra-event scales, and the corresponding quantitative

relationships were established based on a qualifying level of significance ($p < 0.05$) and the

highest coefficient of determination (R^2). Significance levels were set at 95% confidence

intervals. Data analysis was performed using SPSS 21.0, Origin 2018, and Microsoft Excel

2019.

3　Results

3.1 Inter-event variations of rainfall partitioning

3.1.1 Characteristics of inter-event rainfall partitioning variables

A total of 38 rainfall events were recorded for rainfall partitioning measurements, including

20 events (215.4 mm) in 2014 and 18 events (205.6 mm) in 2015, which accounted for 75.2%

300　and 75.0% of total rainfall amount during the experimental period in 2014 and 2015,

respectively (Fig. 2a). The RA ranged from 1.2 to 41.9 mm with an average of 11.1 ± 8.8 mm

(mean ± standard deviation). In general, rainfall events were unevenly distributed in terms of

RA. Approximately 34.2% of rainfall events were smaller than 5 mm, 26.3% within 5-10 mm,

26.3% within 10-20 mm, and 13.2% larger than 20 mm, representing 8.8%, 17.5%, 36.3%,

305　and 37.4% of the total rainfall amount, respectively (Fig. 2a). The average I varied from 0.2

$mm·h^{-1}$ to 35.1 $mm·h^{-1}$ with an average of 6.0 ± 1.3 $mm·h^{-1}$, and approximately 76.3% of the

events was < 5 $mm·h^{-1}$, 13.2% was 5–10 $mm·h^{-1}$, and 10.5% was > 10 $mm·h^{-1}$. I_{10_max}

ranged from 1.2 $mm·h^{-1}$ to 68.4 $mm·h^{-1}$ with an average of 13.7 ± 2.7 $mm·h^{-1}$, and

approximately 42.1% of the events was < 5 $mm·h^{-1}$, 23.7% was 5–10 $mm·h^{-1}$, and 34.2%

310　was > 10 $mm·h^{-1}$. The RD ranged from 0.2 h to 28.9 h and averaged 5.3 ± 1.0 h. The RD of

most rainfall events was less than 5 h (68.4%), and only 5 rainfall events had RD greater than

10 h.

The TF_d for *C. korshinskii* ranged from 0.7 mm to 31.2 mm (coefficient of variation, CV

= 87.5%) with corresponding TF% ranging from 54.0 to 80.3% (CV = 10.6%) across the 38

315　events (Fig. 2b). The TF_d values for *S. psammophila* were 0.4-33.4 mm (CV = 96%) and

28.5-82.7% (CV = 21.5%), respectively (Fig. 2c). The SF_d for *C. korshinskii* ranged from 0.04 mm to 6.1 mm (CV = 106.6%), with corresponding SF % of 2.0-14.5% (CV = 34.2%) (Fig. 2b). The comparable SF_d values for *S. psammophila* varied from 0.01 mm to 2.2 mm (CV = 98.6%) and 0.7-5.9% (CV = 38.9%), respectively (Fig. 2c). The IC_d values for *C.*

320   *korshinskii* varied from 0.5 mm to 2.9 mm (CV = 43.9%), with corresponding IC% of 5.7-40.8% (CV = 47.3%) (Fig. 2b), and the comparable values were 0.8-5.7 mm (CV = 44.8%) and 12.1-70.8% (CV = 53.3%) for *S. psammophila*, respectively (Fig. 2c). For *C. korshinskii*, TF represented the largest component of all rainfall events, while for *S. psammophila*, SF represented the smallest component of all rainfall events (Figs. 2 b and 2c).

325   The percentages of TF, SF, and IC in rainfall partitioning between two species are shown in Fig. 3. There was no significant difference ($p > 0.05$) in average TF% between *C. korshinskii* (69.4 ± 7.4%) and *S. psammophila* (66.7 ± 14.6%). The SF% was significantly higher ($p < 0.05$) for *C. korshinskii* (9.2 ± 3.2%) than *S. psammophila* (3.8 ± 1.5%) (Fig. 3b). The IC% was significantly lower ($p < 0.05$) for *C. korshinskii* (21.4 ± 10.2%) than *S.*

330   *psammophila* (29.5 ± 15.9%) (Fig. 3c). The variations of TF% and IC% among the rainfall events were greater for *S. psammophila*, but that of SF% was smaller compared to *C. korshinskii* (Fig. 3).

3.1.2 Relationships between inter-event rainfall partitioning variables and meteorological factors

335   Correlation analysis indicated that meteorological factors had a similar effect on rainfall partitioning for the two species. Stepwise regression analysis identified that the SF

parameters (SF_d and SF%), TF parameters (TF_d and TF%) and IC parameters (IC_d and IC%) were all mainly controlled by RA. Following RA, the influences of rainfall intensity (I, I_{10_max}) were also significant ($p < 0.05$). However, the other meteorological factors (RD, RI, WS, WD, T, H) had no significant effect on rainfall partitioning ($p > 0.05$).

Significantly positive and linear relationships were found between TF_d and RA for both *C. korshinskii* and *S. psammophila* (Fig. 4a). According to the regression equations, the threshold of rainfall amount for TF generation was 0.8 and 1.1 mm for *C. korshinskii* and *S. psammophila*, respectively. The TF% increased with increasing RA as an exponential function (Fig. 4b). When the RA reached 20 mm, the increasing of TF% became stabilized, and TF% of *C. korshinskii* and *S. psammophila* reached 79.2% and 80.0%, respectively. The SF_d also had a significantly positive and linear relationship with RA for the two species (Fig. 4c). When RA was greater than 1.7 mm and 2.2 mm, *C. korshinskii* and *S. psammophila* began to produce SF, respectively. The SF% increased exponentially with increasing RA, and SF% of *C. korshinskii* was always higher than that of *S. psammophila*. The SF% approximately tended to be constant at 12.2% and 5.5% as RA $\geq$ 20 mm for *C. korshinskii* and *S. psammophila*, respectively (Fig. 4d). The IC_d was also positively correlated with RA (Fig. 4e). However, IC% decreased exponentially with incremental RA, and IC% of *S. psammophila* was always higher than that of *C. korshinskii* (Fig. 4f). When RA reached 20 mm, IC% approximately tended to be constant at 9.0% and 14.5% for *C. korshinskii* and *S. psammophila*, respectively.

3.2 Intra-event variations of rainfall partitioning

3.2.1 Characteristics of intra-event rainfall partitioning variables

The intra-event TF and SF were well synchronized with rainfall process, in terms of the shape, number and location of the intensity peaks for both *C. korshinskii* and *S. psammophila*, which was vividly demonstrated at representative four rainfall events in Fig. 5. The SF intensity (SFI_{10}) was much higher than TF intensity (TFI_{10}) and rainfall intensity (I_{10}) for both *C. korshinskii* and *S. psammophila*, whereas TFI_{10} was less than or equal to I_{10}. As expected, IC was the main component at the initial stage of rainfall, and then TF was the major component ($\geq 50\%$) for rainfall partitioning (Fig. 5). The TF and SF generation thresholds measured using the TBRGs were 0.4 ± 0.2 mm and 1.0 ± 0.7 mm for *C. korshinskii*, and 0.3 ± 0.1 mm and 0.7 ± 0.3 for *S. psammophila*, respectively. They were expected to be both smaller than the thresholds derived from the regression equation between TF_d (or SF_d) and RA aforementioned which assume that TF and SF start after the canopy is fully wet. This further demonstrates the importance of high-resolution data in rainfall partitioning studies.

Fig. 6 describes the difference in average intra-event TF and SF variables between *C korshinskii* and *S. psammophila*. Although there were no statistically significant differences between the two species in intensities, durations, or the lag time of TF and SF, some trends were observed. The TFI and TFI_{10_max} of both species were similar to I (6.0 ± 1.3 mm/h) and I_{10_max} (13.7 ± 2.7 mm/h), respectively. In contrast, SFI and SFI_{10_max} were significantly greater than I and I_{10_max}, respectively. Specifically, TFI and TFI_{10_max} of *C. korshinskii* were 3.8 ± 1.2 mm·h^{-1} and 13.3 ± 4.9 mm·h^{-1}, respectively, which were slightly lower than that of

S. psammophila (4.3 ± 1.5 mm·h^{-1} and 14.6 ± 5.5 mm·h^{-1}, respectively) (Fig. 6a). The SFI and SFI$_{10\_max}$ of *C. korshinskii* (753.8 ± 208.0 mm·h^{-1} and 3627.2 ± 1424.7 mm·h^{-1}, respectively) were higher than those of *S. psammophila* (471.2 ± 170.2 mm·h^{-1} and 1424.8 ± 538.3 mm·h^{-1}, respectively) (Fig. 6b).

Furthermore, a time lag was usually observed between the onset of rainfall and the generation of TF (LG$_{TF}$) and SF (LG$_{SF}$). Similarly, there is a time lag between rainfall and TF or SF in terms of the time to reach maximum intensity (LM) and the time to end (LE). The *S. psammophila* had a shorter lag time than *C. korshinskii* in terms of TF (LG$_{TF}$: 0.1 ± 0.04 h vs. 0.3 ± 0.1 h) and SF production (LG$_{SF}$: 0.7 ± 0.3 h vs. 0.8 ± 0.3 h), and their reaching maximum intensity (LM$_{TF}$: 1.8 ± 0.8 h vs. 2.0 ± 0.6 h; LM$_{SF}$: 2.1 ± 0.7 h vs. 2.2 ± 0.5 h) (Figs. 6c and 6d). However, the *S. psammophila* had longer TF duration (5.2 ± 1.4 h vs. 4.8 ± 1.4 h) and LE$_{TF}$ (0.2 ± 0.1 h vs. 0.1 ± 0.1 h) than *C. korshinskii* (Fig. 6c). Conversely, the SF duration and LE$_{SF}$ in *C. korshinskii* (4.6 ± 1.4 h and 0.4 ± 0.1 h, respectively) were longer than those in *S. psammophila* (4.1 ± 1.3 h and 0.2 ± 0.2 h, respectively) (Fig. 6d). The above differences in TF and SF variables indicate that *S. psammophila* should be more conducive to generate TF than *C. korshinskii*, while *C. korshinskii* should be more conducive to produce SF than *S. psammophila*.

3.2.2 Relationships between intra-event rainfall partitioning variables and meteorological factors

Similar relationships existed between intra-event rainfall partitioning variables and meteorological factors for two species. For both shrubs, rainfall intensity (I, I$_{10\_max}$, and I$_{10\_b}$)

and RD were the main influencing factors affecting intra-event TF variables (Fig. 7) and SF

variables (Fig. 8). While the effects of other meteorological factors (RD, RI, WS, WD, T, H)

on TF and SF variables within the event were not significant ($p > 0.05$). The TFI, TFI_{10_max},

LM_{TF}, and TFD were linearly correlated with I, I_{10_max}, LM_R, and RD, respectively, while

LG_{TF} was power functionally correlated with I_{10_b} ($p < 0.05$). The TF intensities (TFI and

TFI_{10_max}) of *S. psammophila* increased faster with rainfall intensities (I and I_{10_max}) than that

of *C. korshinskii*. The SFI, SFI_{10_max}, LM_{SF}, and SFD were also linearly correlated with I,

I_{10_max}, LM_R, and RD, respectively ($p < 0.05$). The LG_{SF} was power functionally correlated

with I_{10_b} ($p = 0.14$ and $p = 0.16$ for *C. korshinskii* and *S. psammophila*, respectively), which

was weaker than the correlation between LG_{TF} with I_{10_b}. The SF intensities (SFI and

SFI_{10_max}) of *C. korshinskii* increased with rainfall intensities (I and I_{10_max}) more rapidly than

that of *S. psammophila*. However, for both species, there was no significant relationship

between LE_{TF} or LE_{SF} and RD (Figs. 7 and 8). The above results indicate that the intra-event

rainfall partitioning variables largely dependent on rainfall intensity and duration.

4   Discussion

4.1 Rainfall partitioning and influencing factors at inter-event scale

This study indicated that SF% of *C. korshinskii* (9.2%) was significantly higher than that of *S.

psammophila* (3.8%) (Fig. 3), which was comparable to the value of 10.4% and 6.3%

reported by Yang et al. (2019) for the same species in similar semiarid regions of China.

Under the same rainfall regimes, the difference in vegetation characteristics is the main

reason for the difference in SF (Yuan et al., 2017; Whitworth-Hulse et al., 2020a; Yue et al.,

420   2021). Comparing the structural properties of two shrubs with the same age (20 years), we

found that CA, BD, BL, BA and NB values of *S. psammophila* were 4.51, 1.61, 1.94, 0.83

and 1.52 times of those of *C. korshinskii*, respectively (Table 1). On the branch scale, *C.*

korshinskii had more small and short branches, but larger BA than that of *S. psammophila*,

which was contributed to SF generation. Yuan et al. (2016) concluded that a beneficial branch

425   architecture for SF production should include more relatively small branches and larger

branch angles, and SF productivity decreased with BD size of branches. Furthermore, *C.*

korshinskii with a smaller CA, and it had a larger SF_d than *S. psammophila* under the

same SF volume. Somewhat in line with Yuan et al. (2016) and Yue et al. (2021), our

results suggest that a beneficial branch architecture for SF production of *C. korshinskii* should

430   include relatively small CA, BD, BL and large BA (Table 1).

    Leaf traits had been reported to exert a significant influence on rainfall partitioning

(Garcia-Estringana et al., 2010; Magliano et al., 2019a). According to the documentation in

Flora of China (Liu et al., 2010), *C. korshinskii* has pinnate compound leaves and each pinna

has 5 to 8 pairs of ovate leaflets, and the leaves are lanceolate and concave, and the surface is

435   densely sericeous. In comparison, *S. psammophila* has stripe or stripe oblanceolate leaves,

margin revolute, and which upper surface of mature leaf blade is almost glabrous (Chao and

Gong, 1999). The branches of both shrubs are smooth, with a more developed cuticle layer on

the surface of the *S. psammophila* branches, while the *C. korshinskii* branches contain oil and

have waxy skin (Chao and Gong, 1999; Liu et al., 2010). The leaf morphology and epidermal

440   characteristics of branches of *C. korshinskii* was more beneficial for SF generation than that

of *S. psammophila* (Whitworth-Hulse et al., 2020b; Yuan et al. 2017). It was found that big biomass of leaves, concave leaf shape and leaf pubescence are beneficial to promote the generation of SF (Yuan et al., 2016). These factors together enable the leaves to function as a highly efficient natural water collecting system.

445 The mean IC% of *C. korshinskii* (21.4%) was significantly lower than that of *S. psammophila* (29.5%) in this study. The intercepts in the fitted formulas between interception loss and rainfall amount in Fig. 4e indicated that *C. korshinskii* (0.92 mm) had a lower canopy water storage than *S. psammophila* (1.15 mm), hence the potential interception loss of *C. korshinskii* was lower. Zhang et al. (2017) reported that IC% were higher in the *H. rhamnoides* stand (24.9%) than in the *S. pubescens* stand (19.2%), which was mainly attributed to the lower canopy water storage of *S. pubescen*. This study was done at the shrub-scale, so we compared the total canopy water storage of individual plant (C_m), and we found that C_m of *S. psammophila* (6.0 L) was significantly higher than that of *C. korshinskii* (3.9 L) (Table 1). This was mainly due to the significantly higher average total dry aboveground biomass of *S. psammophila* (15.7 kg per plant) than *C. korshinskii* (4.6 kg per plant). Consequently, individual *S. psammophila* absorbed more rain water to moisten the branches and leaves than that of individual *C. korshinskii*, which could explain higher IC% of *S. psammophila* than *C. korshinskii*. Thus, the best predictors for interception loss were biomass-related parameters (i.e., woody biomass and total biomass) (Li et al., 2016).

460 **4.2 Rainfall partitioning and influencing factors at intra-event scale**

Temporal heterogeneity of rainfall clearly influences the amount and timing of TF and SF

reaching the soil under the canopy, as explained by some previous intra-event rainfall partitioning studies from forested ecosystems (Owens et al., 2006; Levia et al., 2010; Molina et al., 2019). Our experiment investigated the intra-event dynamics of all rainfall partitioning components in xerophytic shrubs, which has scarily been reported before. Our results showed that the temporal dynamics of TF and SF under the shrub canopy almost matched the dynamics of rainfall (Fig. 5). It agreed with the reports of Zhang et al. (2018) and Yuan et al. (2019) who demonstrated the temporal synchronization of TF and SF with rainfall, respectively. The SF intensity is generally greater than rainfall intensity for different species (Fig. 6), which can influence ecohydrological processes such as groundwater recharge, erosion, and overland flow (Spencer and van Meerveld, 2016). The SF converges substantial rainwater to the shrub bases and then delivers it into the soil as a point input to recharge soil moisture and nutrient enrichment (Germer et al., 2010; Wang et al., 2011; Cayuela et al., 2018; Jian et al., 2019). Moreover, as stemflow water is funneled belowground along roots of the shrubs (Martinez-Meza and Whitford, 1996; Li et al., 2009), we suggest that changes in SF inputs explain, at least in part, the temporal variation in subsurface moisture patterns.

The intensity variables and lag time of SF and TF relative to rainfall were the key to describe the intra-event rainfall partitioning (Fig. 6). The effects of meteorological factors on SF and TF variables at the intra-event scale were derived from multiple regression analysis in this study. The SF and TF variables (intensity and temporal dynamics) were strongly influenced by rainfall intensity (e.g., I, I_{10_max} and I_{10_b}) and duration (e.g., RD and LM_R). This is consistent with the results reported by Yuan et al. (2019) who indicated that there was

a significant effect of rainfall intensity on the stemflow process of *C. korshinskii*. The main factors affecting intra-event SF and TF variables were the same, but the effects were still slightly different between the two shrubs. Under the same rainfall intensity, the average TF intensity under the canopy of *S. psammophila* was higher than *C. korshinskii* (Figs. 7a and 7b). But the average SF intensity of *C. korshinskii* was greater than *S. psammophila* at shrub scale (Figs. 8a and 8b), which was also found for the branch SF intensity reported by Yuan et al. (2019). In addition to the inter-shrub differences, the effects of I_{10_b} on LG_{TF} and LG_{SF} were slightly different. The correlation between LG_{SF} and I_{10_b} (Fig. 8c) was weaker than that between LG_{TF} and I_{10_b} (Fig. 7c). This may be due to the fact that TF has two components, i.e., free TF and released TF (Staelens et al., 2008; Levia et al., 2017; Van Stan II et al., 2020), and that SF only starts to produce when a certain amount of rainfall is reached (Germer et al., 2010; Levia et al., 2010; Dunkerley, 2014; Yuan et al., 2019). Our results indicated that *S. psammophila* had dynamic characteristics (e.g., larger TFI, TFI_{10} and LE_{TF} as well as TFD, and shorter LG_{TF} and LM_{TF}) producing larger TF depth (TFd = TFI*TFD) (Figs. 6a and 6c), while *C. korshinskii* had dynamic characteristics (e.g., larger SFI, SFI_{10} and LE_{SF} as well as SFD) producing larger SF depth (SFd = SFI*SFD) (Figs. 6b and 6d).

The vegetation characteristics have an important effect on the dynamics and the lag time of TF and SF (Yuan et al., 2019; Zhang et al., 2018). Based on the temporal data recorded by TBRGs, we found that *C. korshinskii* produced TF and SF later than *S. psammophila* (Figs. 5 and 6), which was also reported by Yuan et al. (2019) for branch SF of the same species. We inferred that this was due to the higher canopy water storage capacity of *C. korshinskii* (0.85

mL/g) compared to *S. psammophila* (0.38 mL/g). However, when the branches were

moistened, SF production of *C. korshinskii* was greater than that of *S. psammophila* because

of its branch and leaf characteristics as discussed in subsection 4.1 (Fig. 5). It was found that

the great bark water storage capacity of forests could result in the further delay of TF and SF

onset (Levia and Herwitz, 2005; Levia et al., 2010; Li et al., 2016; Pinos et al., 2021). In

summary, the different intra-event TF and SF dynamics between species were attributed to a

complex interaction of biotic and abiotic factors (Yuan et al., 2019; Zhang et al., 2018; Levia

et al., 2010).

4.3 Implications and further scopes

Most of previous rainfall partitioning investigations for shrubs were limited at inter-event scale,

or only focused on TF or SF at intra-event scale. The intra-event rainfall partitioning dynamics,

which could help have a better understanding of soil water replenishment and its distribution in

soil and the key ecohydrological cycle in in drylands, have been rarely explored. This study is

the first time to investigate all the rainfall partitioning components (i.e., TF, SF and IC) for

shrubs at both inter- and intra-event scales, which steps further and provides a full view of the

reciprocal dynamics among interception loss, throughfall, and stemflow at the shrub-scale.

This is the main novelty and a step forward compared with the previous related studies. We

have also obtained the quantitative relationship between rainfall partitioning variables and

rainfall characteristics, and further elaborated the influence of vegetation structure

characteristics (leaf, canopy structure, and biomass, etc..) on rainfall partitioning. The obtained

new insights help to understand the fine characterization of shrub-dominated eco- hydrological

525 processes, and improve the accuracy of water balance estimation in dryland ecosystem.

There are several issues that need further investigation. Firstly, long-term observations of rainfall partitioning dynamics for more shrub plants and species are needed, and the rainfall partitioning models should be developed for shrubs. Every component of shrub canopy water balance including canopy evaporation loss and transpiration should be considered. Secondly,

530 the effects of rainfall partitioning on soil moisture dynamics, nutrient cycling, and plant transpiration should be substantially investigated. How the shrubs actually make use of small amounts of throughfall or stemflow should be examined to detect the interactions between water redistribution and vegetation physiological processes. Finally, the extension from the individual plant to stand and larger scales remains a challenging topic for rainfall partitioning,

535 which can help improve understanding the role of rainfall partitioning in the regional hydrologic cycle.

5   Conclusions

In this study, we analyze the rainfall partitioning and the influences of bio-/abiotic factors of two typical shrubs at both inter- and intra-event scales in the Loess Plateau. To ensure a larger

540 proportion of the rainfall is allocated under the canopy, two species can obtain more net rainfall through different mechanisms. At the event scale, there was no significant difference in TF percentage between the two shrubs, but *C. korshinskii* had significantly higher SF percentage and lower IC percentage compared to *S. psammophila*. At the intra-event scale, TF and SF of two shrubs were well synchronized with the rainfall, but *C. korshinskii* had the advantage of

545 stemflow production, while *S. psammophila* had the advantage of TF generation. For both

shrubs, the inter-event rainfall partitioning amount and percentage depended more on rainfall amount, and rainfall intensity and duration controlled the intra-event TF and SF variables. The *C. korshinskii* has larger branch angles, more small branches and smaller canopy areas to produce SF more efficiently, and *S. psammophila* has larger biomass to intercept more rainfall

550   amount. These findings could enhance our understanding of TF and SF dynamics and corresponding driving factors at inter- and intra-event scales, and help in modelling the critical eco-hydrological processes in arid and semi-arid regions.

Data availability: The data that support the findings of this study are available from the

555   corresponding author upon request.

Author contributions: JXA: Formal analysis, Investigation, Methodology, Writing - original draft; GYG: Conceptualization, Methodology, Writing - review & editing; CY: Investigation, Writing - review & editing; JP and BJF: Writing - review & editing.

560

Competing interests: The authors declare that they have no conflict of interest.

565

References

Cayuela, C., Llorens, P., Sanchez-Costa, E., Levia, D. F., and Latron, J.: Effect of biotic and abiotic factors on inter- and intra-event variability in stemflow rates in oak and pine stands in a Mediterranean mountain area, J. Hydrol., 560, 396-406, 2018.

Chao, P. N. and Gong, G. T.: *Salix* (*Salicaceae*), in: Flora of China, edited by: Wu, Z. Y., Raven, P. H., and Hong, D. Y., Science Press, Beijing and Missouri Botanical Garden Press, St. Louis, 162–274, 1999.

Chesson, P., Gebauer, R. L., Schwinning, S., Huntly, N., Wiegand, K., Ernest, M. S., Sher, A., Novoplansky, A., and Weltzin, J. F.: Resource pulses, species interactions, and diversity maintenance in arid and semi-arid environments, Oecologia, 141, 236-253, 2004.

Chu, X., Han, G., Xing, Q., Xia, J., Sun, B., Yu, J. B., and Li, D.: Dual effect of precipitation redistribution on net ecosystem CO_2 exchange of a coastal wetland in the Yellow River Delta, Agr. Forest Meteorol., 249, 286-296, 2018.

Dunkerley, D.: Stemflow production and intrastorm rainfall intensity variation: an

570

575

580

experimental analysis using laboratory rainfall simulation, Earth. Surf. Proc. Land., 39,

585 1741-1752, 2014.

Garcia-Estringana, P., Alonso-Blázquez, N., and Alegre, J.: Water storage capacity, stemflow

and water funneling in Mediterranean shrubs, J. Hydrol., 389, 363-372, 2010.

Germer, S., Werther, L., and Elsenbeer, H.: Have we underestimated stemflow? Lessons from

an open tropical rainforest, J. Hydrol., 395, 169-179, 2010.

590 Gordon, D. A., Coenders-Gerrits, M., Sellers, B. A., Sadeghi, S. M. M. and Van Stan II, J. T.:

Rainfall interception and redistribution by a common North American understory and

pasture forb, Eupatorium capillifolium (Lam. dogfennel), Hydrol. Earth. Syst. Sci., 24,

4587–4599, 2020.

Hanchi, A., and Rapp, M.: Stemflow determination in forest stands, Forest Ecol. Manage., 97,

595 231-235, 1997.

Honda, E. A., Mendonça, A. H., and Durigan, G.: Factors affecting the stemflow of trees in the

Brazilian Cerrado, Ecohydrology, 8, 1351-1362, 2015.

Iida, S., Shimizu, T., Kabeya, N., Nobuhiro, T., Tamai, K., Shimizu, A., Ito, E., Ohnuki, Y., Abe,

T., Tsuboyama, Y., Chann, S., and Keth, N.: Calibration of tipping-bucket flow meters and

600 rain gauges to measure gross rainfall, throughfall, and stemflow applied to data from a

Japanese temperate coniferous forest and a Cambodian tropical deciduous forest, Hydrol.

Process., 26, 2445-2454, 2012.

Jia, X. X., Shao, M. A., Wei, X. R., and Wang, Y. Q.: Hillslope scale temporal stability of soil

water storage in diverse soil layers, J. Hydrol., 498, 254-264, 2013.

605   Jia, X., Zha, T. S., Gong, J. N., Wang, B., Zhang, Y. Q., Wu, B., Qin, S. G., and Peltola, H.:

Carbon and water exchange over a temperate semi-arid shrubland during three years of

contrasting precipitation and soil moisture patterns, Agr. Forest Meteorol., 228, 120-129,

2016.

Jian, S. Q., Hu, C. H., Zhang, G. D., and Zhang, J. P.: Study on the throughfall, stemflow, and

610   interception of two shrubs in the semiarid Loess region of China, Agr. Forest Meteorol.,

279, 107713, 2019.

Lacombe, G., Valentin, C., Sounyafong, P., de Rouw, A., Soulileuth, B., Silvera, N., Pierret, A.,

Sengtaheuanghoung, O., and Ribolzi, O.: Linking crop structure, throughfall, soil surface

conditions, runoff and soil detachment: 10 land uses analyzed in Northern Laos, Sci. Total

615   Environ., 616-617, 1330-1338, 2018.

Levia, D. F. and Frost, E. E.: A review and evaluation of stemflow literature in the hydrologic

and biogeochemical cycles of forested and agricultural ecosystems, J. Hydrol., 274, 1-29,

2003.

Levia, D. F. and Germer, S.: A review of stemflow generation dynamics and

620   stemflow-environment interactions in forests and shrublands, Rev. Geophys., 53, 673-714,

2015.

Levia, D.F. and Herwitz, S. R.: Interspecific variation of bark water storage capacity of three

deciduous tree species in relation to stemflow yield and solute flux to forest soils, Catena,

64, 117-137, 2005.

625   Levia, D.F.,Hudson, S. A., Llorens, P., and Nanko, K.: Throughfall drop size distributions: a

review and prospectus for future research, WIREs Water, 4, 2017.

Levia, D. F., Van Stan II, J. T., Mage, S. M., and Kelley-Hauske, P. W.: Temporal variability of stemflow volume in a beech-yellow poplar forest in relation to tree species and size, J. Hydrol., 380, 112-120, 2010.

630   Li, X., Xiao, Q. F., Niu, J. Z., Dymond, S., van Doorn, N. S., Yu, X. X., Xie, B. Y., Lv, X. Z., Zhang, K. B., and Li, J.: Process-based rainfall interception by small trees in Northern China: The effect of rainfall traits and crown structure characteristics, Agr. Forest Meteorol., 218-219, 65-73, 2016.

Li, X. Y., Yang, Z. P., Li, Y. T., and Lin, H.: Connecting ecohydrology and hydropedology in

635   desert shrubs: stemflow as a source of preferential flow in soils, Hydrol. Earth. Syst. Sci., 13, 1133-1144, 2009.

Liu, Y. X., Chang, Z. Y. and Gennady, P. Y.: *Caragana* (*Fabaceae*), in: Flora of China, edited by: Wu, Z. Y., Raven, P. H., and Hong, D. Y., Science Press, Beijing and Missouri Botanical Garden Press, St. Louis, 528–545, 2010.

640   Llorens, P. and Domingo, F.: Rainfall partitioning by vegetation under Mediterranean conditions. A review of studies in Europe, J. Hydrol., 335, 37-54, 2007.

Magliano, P. N., Whitworth-Hulse, J. I., and Baldi, G.: Interception, throughfall and stemflow partition in drylands: Global synthesis and meta-analysis, J. Hydrol., 568, 638-645, 2019a.

645   Magliano, P. N., Whitworth-Hulse, J. I., Florio, E. L., Aguirre, E. C., and Blanco, L. J.: Interception loss, throughfall and stemflow by Larrea divaricata: The role of rainfall

characteristics and plant morphological attributes, Ecol. Res., 34, 753-764, 2019b.

Martinez-Meza, E., Whitford, W. G.: Stemflow, throughfall and channelization of stemflow by roots in three Chihuahuan desert shrubs, J. Arid Environ., 32, 271-287, 1996.

650 Molina, A. J., Llorens, P., Garcia-Estringana, P., Moreno de Las Heras, M., Cayuela, C., Gallart, F., and Latron, J.: Contributions of throughfall, forest and soil characteristics to near-surface soil water-content variability at the plot scale in a mountainous Mediterranean area, Sci. Total Environ., 647, 1421-1432, 2019.

Owens, M. K., Lyons, R. K., and Alejandro, C. L.: Rainfall partitioning within semiarid juniper

655 communities: effects of event size and canopy cover, Hydrol. Process., 20, 3179-3189, 2006.

Pinos, J., Latron, J., Levia, D. F., and Llorens, P.: Drivers of the circumferential variation of stemflow inputs on the boles of Pinus sylvestris L. (Scots pine), Ecohydrology, 14, e2348, 2021.

660 Rivera, D. N. and Van Stan II, J. T.: Grand theft hydro? Stemflow interception and redirection by neighbouring Tradescantia ohiensis Raf. (spiderwort) plants, Ecohydrology, 13, e2239, 2020.

Sadeghi, S. M. M., Gordon, D. A., and Van Stan II, J. T.: A Global Synthesis of Throughfall and Stemflow Hydrometeorology. In: Van Stan II, J. T., Gutmann, E., Friesen, J. (Eds.),

665 Precipitation Partitioning by Vegetation, Springer Nature Switzerland, Cham, pp. 49-70, 2020.

Soulsby, C., Braun, H., Sprenger, M., Weiler, M., and Tetzlaff, D.: Influence of forest and shrub

canopies on precipitation partitioning and isotopic signatures, Hydrol. Process., 31, 4282-4296, 2017.

670   Spencer, S. A. and van Meerveld, H. J.: Double funnelling in a mature coastal British Columbia Forest: spatial patterns of stemflow after infiltration, Hydrol. Process., 30, 4185-4201, 2016.

Staelens, J., De Schrijver, A., Verheyen, K., and Verhoest, N.E.C.: Rainfall partitioning into throughfall, stemflow, and interception within a single beech (Fagus sylvatica L.) canopy:

675   influence of foliation, rain event characteristics, and meteorology, Hydrol. Process., 22, 33-45, 2008.

Tonello, K. C., Rosa, A. G., Pereira, L. C., Matus, G. N., Guandique, M. E. G., and Navarrete, A. A.: Rainfall partitioning in the Cerrado and its influence on net rainfall nutrient fluxes, Agr. Forest Meteorol., 303, 108372, 2021.

680   Van Stan II, J. T., Gutmann, E., and Friesen, J. (Eds.): Precipitation Partitioning by Vegetation — A Global Synthesis, Precipitation Partitioning by Vegetation, Springer Nature Switzerland, 2020.

Van Stan II, J. T., Wagner, S., Guillemette, F., Whitetree, A., Lewis, J., Silva, L., and Stubbins, A.: Temporal dynamics in the concentration, flux, and optical properties of tree-derived

685   dissolved organic matter in an epiphyte-laden oak-cedar forest, J. Geophys. Res.-Biogeosci., 122, 2982-2997, 2017.

Wang, X. P., Zhang, Y. F., Hu, R., Pan, Y. X., and Berndtsson, R.: Canopy storage capacity of xerophytic shrubs in Northwestern China, J. Hydrol., 454, 152-159, 2012.

Wang, X., Wang, Z., Berndtsson, R., Zhang, Y., and Pan, Y.: Desert shrub stemflow and its

690   significance in soil moisture replenishment, Hydrol. Earth. Syst. Sci., 15, 561-567, 2011.

Whitworth-Hulse, J. I., Magliano, P. N., Zeballos, S. R., Gurvich, D. E., Spalazzi, F., and

Kowaljow, E.: Advantages of rainfall partitioning by the global invader Ligustrum

lucidum over the dominant native Lithraea molleoides in a dry forest, Agr. Forest

Meteorol., 290, 108013, 2020a.

695 Whitworth-Hulse, J. I., Magliano, P. N., Zeballos, S. R., Aguiar, S., and Baldi, G.: Global

patterns of rainfall partitioning by invasive woody plants, Global Ecol. Biogeogr., 30,

235-246, 2020b.

Xu, H. and Li, Y.: Water-use strategy of three central Asian desert shrubs and their responses to

rain pulse events, Plant and Soil, 285, 5-17, 2006.

700 Yang, X. L., Shao, M. A., and Wei, X. R.: Stemflow production differ significantly among tree

and shrub species on the Chinese Loess Plateau, J. Hydrol., 568, 427-436, 2019.

Yuan, C., Gao, G. Y., and Fu, B. J.: Stemflow of a xerophytic shrub (Salix psammophila) in

northern China: Implication for beneficial branch architecture to produce stemflow, J.

Hydrol., 539, 577-588, 2016.

705 Yuan, C., Gao, G. Y., and Fu, B. J.: Comparisons of stemflow and its bio-/abiotic influential

factors between two xerophytic shrub species, Hydrol. Earth. Syst. Sci., 21, 1421-1438,

2017.

Yuan, C., Gao, G. Y., Fu, B. J., He, D. M., Duan, X. W., and Wei, X. H.: Temporally dependent

effects of rainfall characteristics on inter- and intra-event branch-scale stemflow

variability in two xerophytic shrubs, Hydrol. Earth. Syst. Sci., 23, 4077-4095, 2019.

Yue, K., De Frenne, P., Fornara, D. A., Van Meerbeek, K., Li, W., Peng, X., Ni, X., Peng, Y., Wu, F., Yang, Y., and Penuelas, J.: Global patterns and drivers of rainfall partitioning by trees and shrubs, Glob Chang Biol, 27, 3350-3357, 2021.

Zhang, H., Fu, C., Liao, A., Zhang, C., Liu, J., Wang, N., and He, B.: Exploring the stemflow dynamics and driving factors at both inter- and intra-event scales in a typical subtropical deciduous forest, Hydrol. Process., 35, e14091, 2021a.

Zhang, Y., Li, X. Y., Li, W., Wu, X. C., Shi, F. Z., Fang, W. W., and Pei, T. T.: Modeling rainfall interception loss by two xerophytic shrubs in the Loess Plateau, Hydrol. Process., 31, 1926-1937, 2017.

Zhang, Y. F., Wang, X. P., Hu, R., and Pan, Y. X.: Meteorological influences on process-based spatial-temporal pattern of throughfall of a xerophytic shrub in arid lands of northern China, Sci. Total Environ., 619-620, 1003-1013, 2018.

Zhang, Y. F., Wang, X. P., Pan, Y. X., and Hu, R.: Variations of nutrients in gross rainfall, stemflow, and throughfall within revegetated desert ecosystems, Water Air Soil Pollut., 227, 183, 2016.

Zhang, Y. F., Wang, X. P., Pan, Y. X., Hu, R., Chen, N., and Sandel, R. O.: Global quantitative synthesis of effects of biotic and abiotic factors on stemflow production in woody ecosystems, Global Ecol. Biogeogr., 30, 1713-1723, 2021b.

730 **Table 1.** Descriptive statistics (mean ± standard error) of canopy morphology of *C. korshinskii* (CK1-CK3) and *S. psammophila* (SP1-SP3) plants. Values are mean ± SD.

Plant ID	SH (m)	CA (m^2)	NB	BL (cm)	BA (°)	BD (mm)	TBA (cm^2)	TB (kg)	C_m (L)
CK1	2.2	5.3	47	150.6±5.1	60.26±2.6	9.2±0.5	34.9	4.0	3.4
CK2	2.3	5.2	47	123.3±6.6	65.5±2.1	8.5±0.5	31.3	3.6	3.1
CK3	2.4	5.3	49	134.6±6.7	65.4±4.4	9.9±0.7	45.8	6.2	5.2
Average	2.3a	5.27a	48a	136.2a	63.77a	9.2a	37.3a	4.6a	3.9a
SP1	3.5	23.9	85	262.2±6.0	67.1±1.4	13.8±0.5	139.7	14.3	5.4
SP2	3.3	26.1	55	268.0±7.7	56.0±3.1	15.1±0.6	124.3	15.9	6.0
SP3	3.6	21.4	78	262.0±7.8	35.1±2.9	15.3±0.5	155.9	17.0	6.5
Average	3.5b	23.8b	73b	264.1b	52.7a	14.8b	140.0b	15.7b	6.0b

Note: SH: shrub height; CA: canopy area; NB: number of branches; BL: branch length; BA: branch angle; BD: basal diameter of branch; TBA: total basal area of the shrub; TB: total dry aboveground biomass; C_m: total canopy storage per plant. Different letters indicate statistically significant differences between two

735 species ($p < 0.05$).

Table 2. Rainfall partitioning parameters at inter- and intra-event scales.

| Scale	Parameter (unit)	Explanation
Inter-event	TF_d (mm)	Throughfall depth per rainfall event
	SF_d (mm)	Stemflow depth per rainfall event
	IC_d (mm)	Interception loss depth per rainfall event
	TF%	Percentage of TF per rainfall event
	SF%	Percentage of SF per rainfall event
	IC%	Percentage of IC per rainfall event
	TFD (h)	Throughfall duration
	SFD (h)	Stemflow duration
	TFI (mm·h^{-1})	Average throughfall intensity
	SFI (mm·h^{-1})	Average stemflow intensity
Intra-event	I_{10} (mm·h^{-1})	Rainfall intensity at 10-min interval
	I_{10_max} (mm·h^{-1})	Maximum I_{10} during the rainfall process
	TFI_{10} (mm·h^{-1})	Throughfall intensity at 10-min interval
	TFI_{10_max} (mm·h^{-1})	Maximum TFI_{10} during the rainfall process
	SFI_{10} (mm·h^{-1})	Stemflow intensity at 10-min interval
	SFI_{10_max} (mm·h^{-1})	Maximum SFI_{10} during the rainfall process
	LG_{TF} (h)	Time lag of throughfall generation after the start of rainfall
	LG_{SF} (h)	Time lag of stemflow generation after the start of rainfall
	LM_R (h)	Time lag of I_{10_max} occurrence relative to the onset of rainfall
	LM_{TF} (h)	Time lag of TFI_{10_max} occurrence relative to the onset of rainfall
	LM_{SF} (h)	Time lag of SFI_{10_max} occurrence relative to the onset of rainfall
	LE_{SF} (h)	Time lag of throughfall ending after the end of rainfall
	LE_{SF} (h)	Time lag of stemflow ending after the end of rainfall
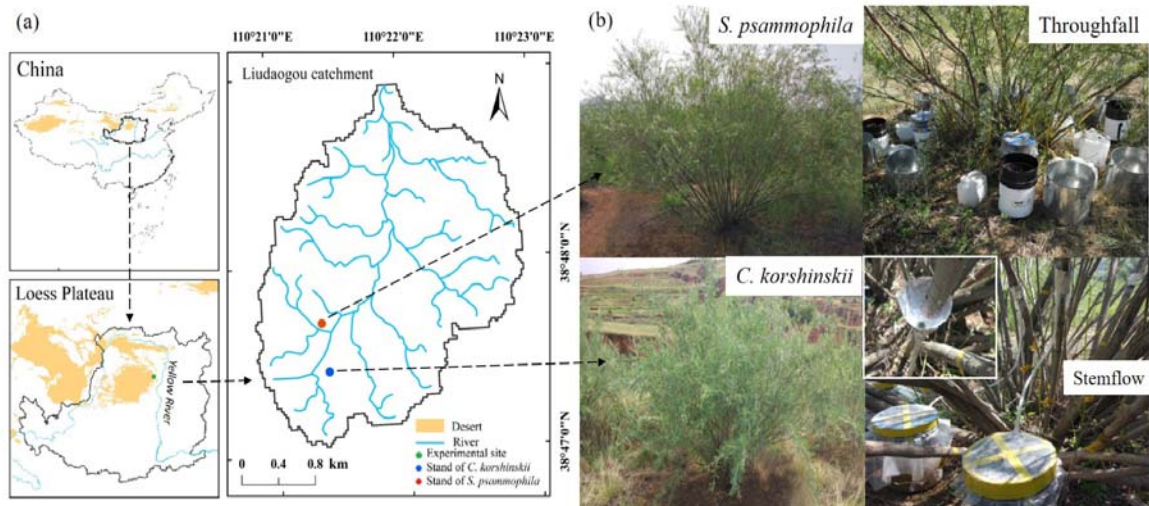
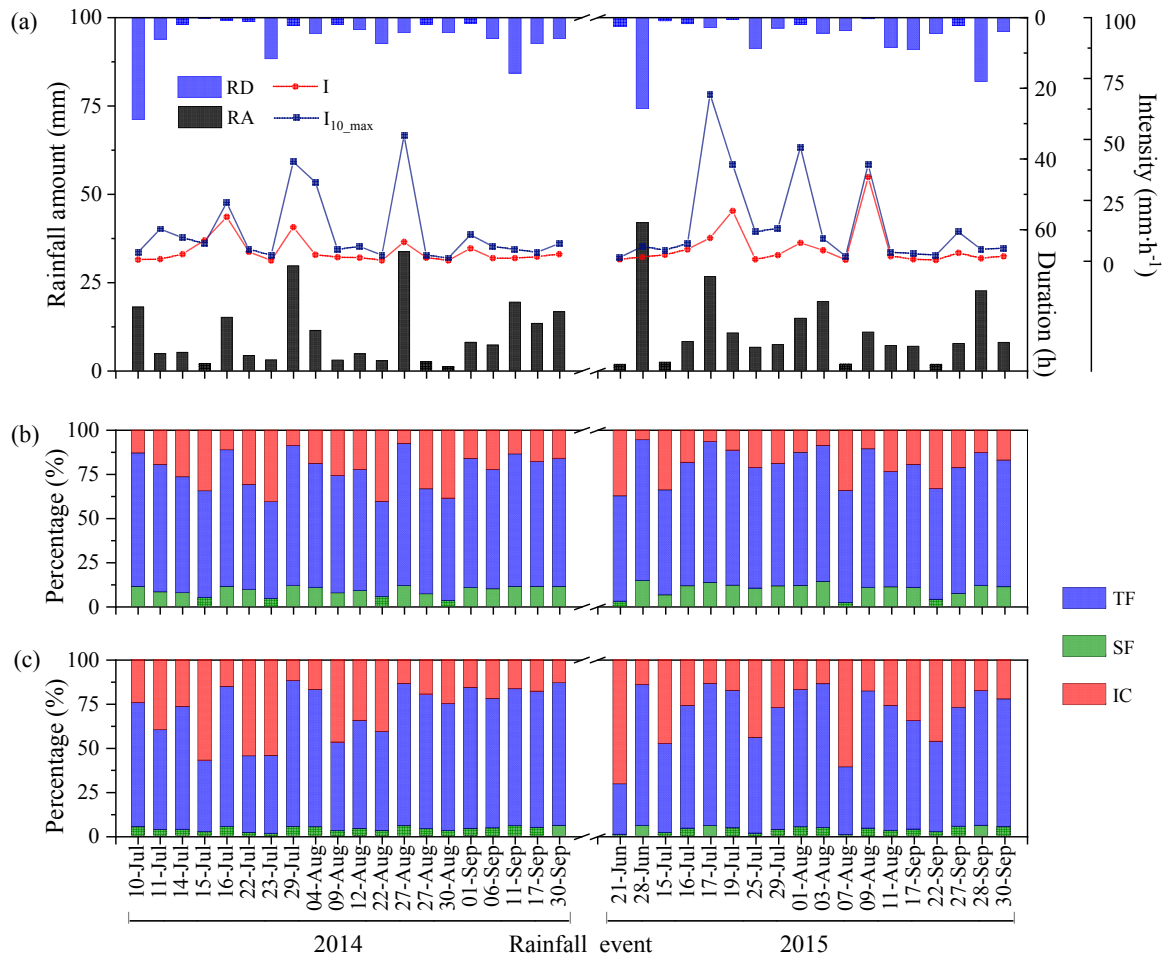**Figure 1.** The location and experimental settings in the plots of *C. korshinskii* and *S. psammophila.*

Figure 2. (a) individual rainfall amount (RA) ($n = 38$), rainfall duration (RD), average rainfall intensity (I, mm·h^{-1}), maximum rainfall intensity at 10-min interval (I$_{10\_max}$, mm·h^{-1}); and rainfall partitioning into TF %, SF %, and IC % of (b) *C. korshinskii* and (c) *S. psammophila*.
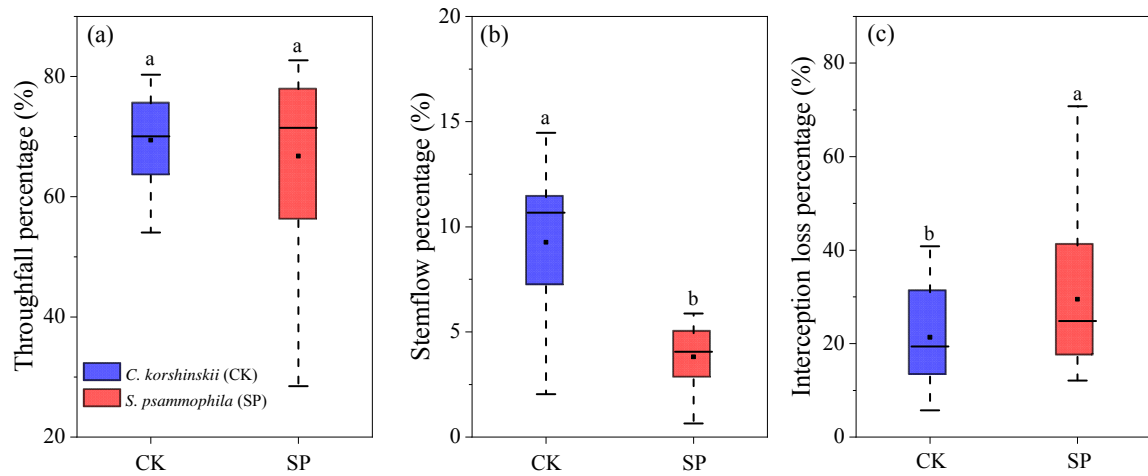
Figure 3. Box-plots of (a) TF%, (b) SF%, and (c) IC% for *C. korshinskii* (CK) and *S. psammophila* (SP). The horizontal thick black line indicates the median, boxes correspond to the 25th and 75th percentiles, and whiskers represent values that fall within 1.5 times the interquartile range. Mean values are represented with the black square. Different letters indicate significant differences between the two species ($p < 0.05$).
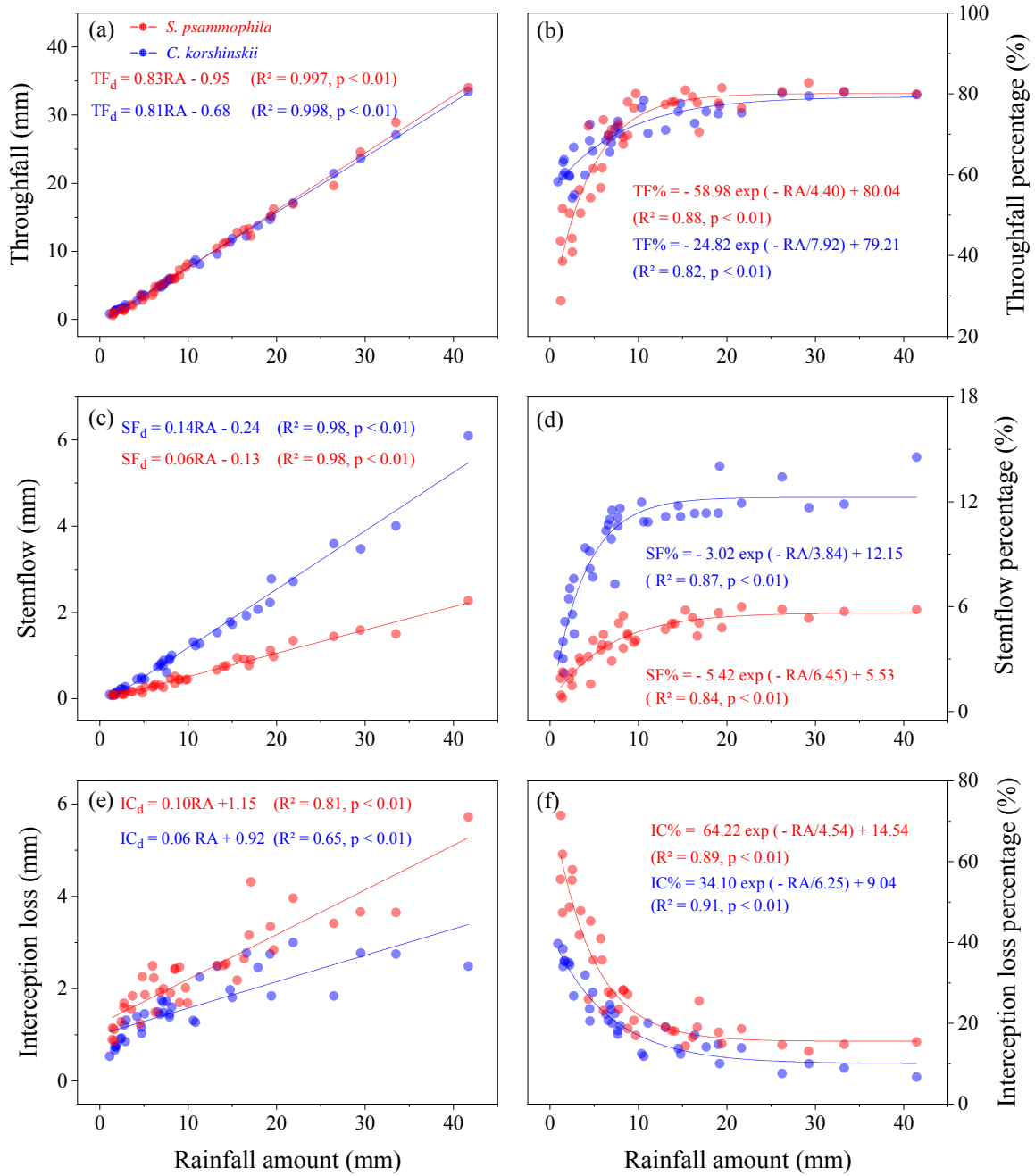
755

Figure 4. Inter-event rainfall partitioning as a function of individual rainfall amount for *C. korshinskii* and *S. psammophila*.
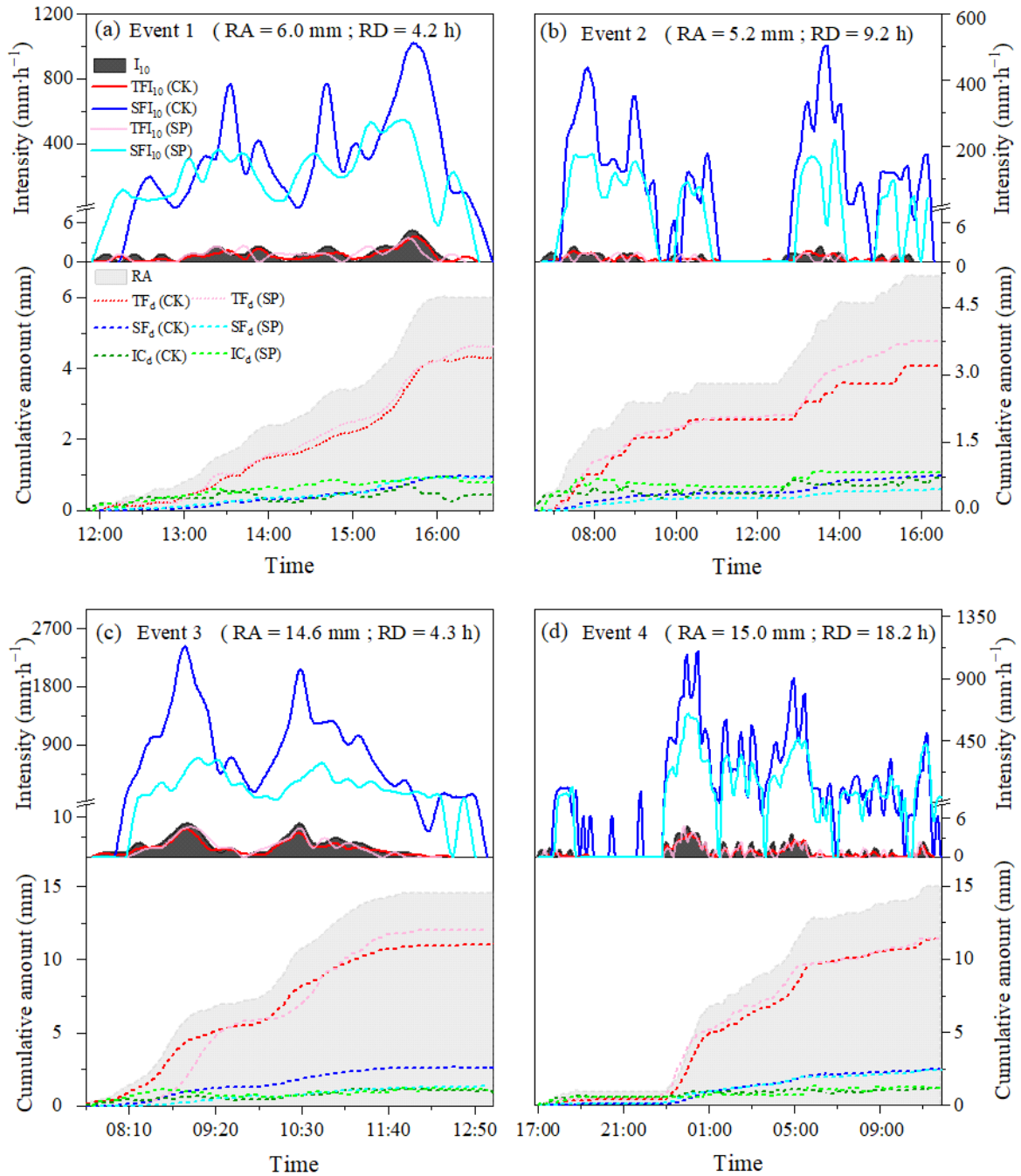
Figure 5. Time series (10-min interval) of rainfall partitioning within four rainfall events for *C. korshinskii* (CK) and *S. psammophila* (SP). Events 1-4 occurred on August 3, September 17, September 28, and September 30 in 2015, respectively. The solid lines represent the rainfall, TF and SF intensity at 10-min interval. The dotted lines indicate the accumulated amount of RA, TF, SF, and IC.
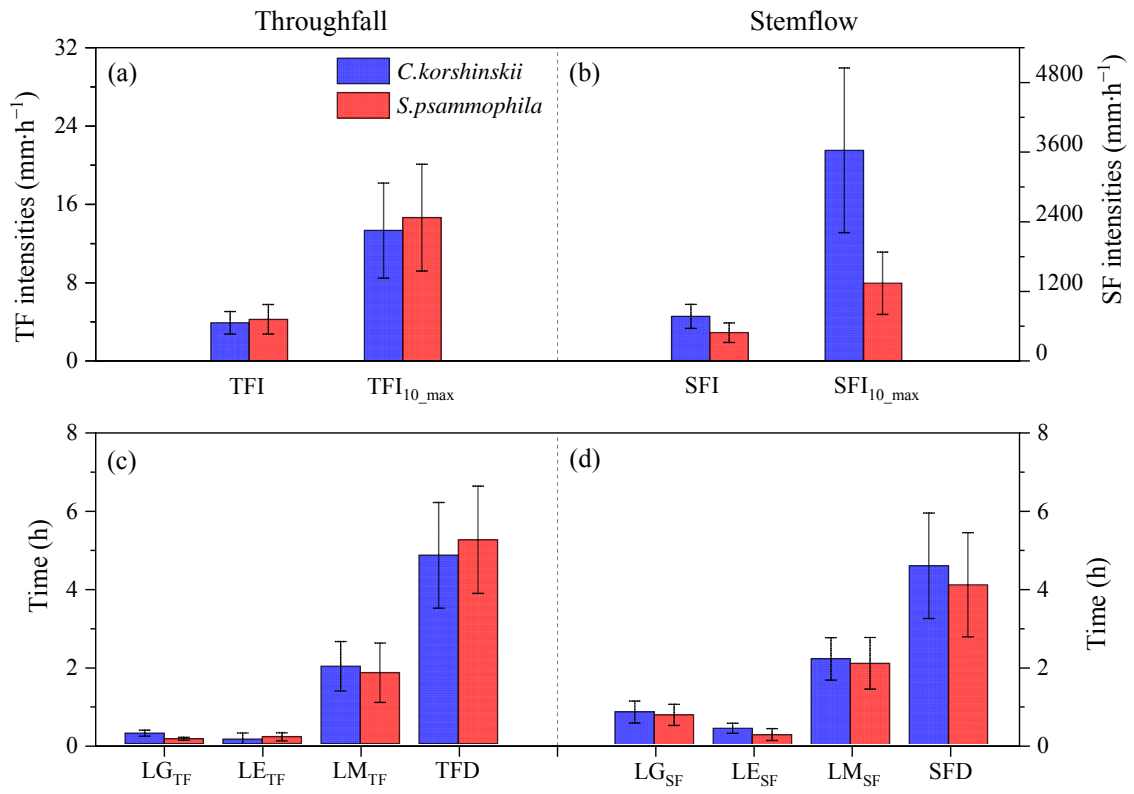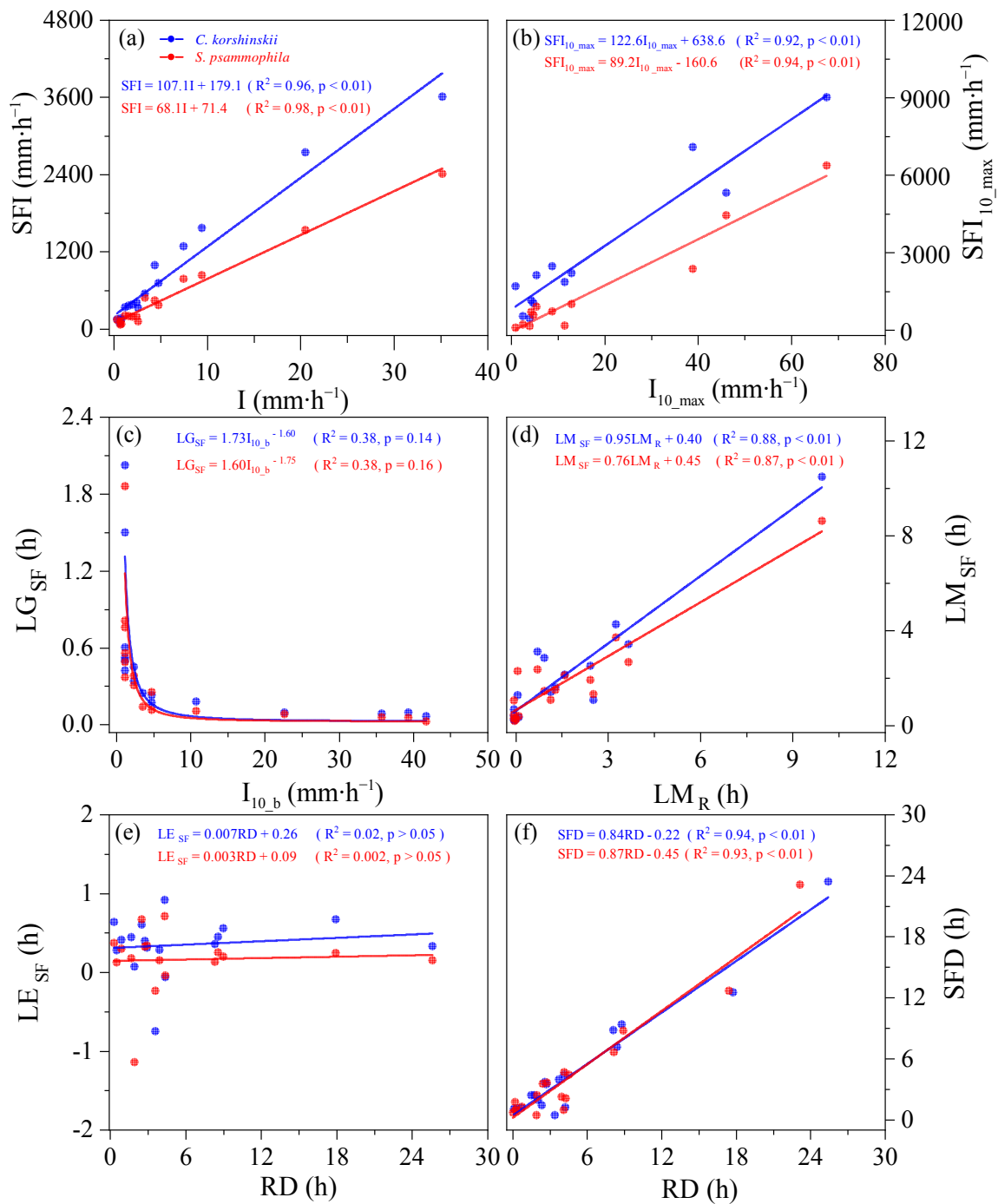
765

Figure 6. Intra-event TF (a, c) and SF (b, d) variables of *C. korshinskii* and *S. psammophila.*

All the variables are explained in Table 2.
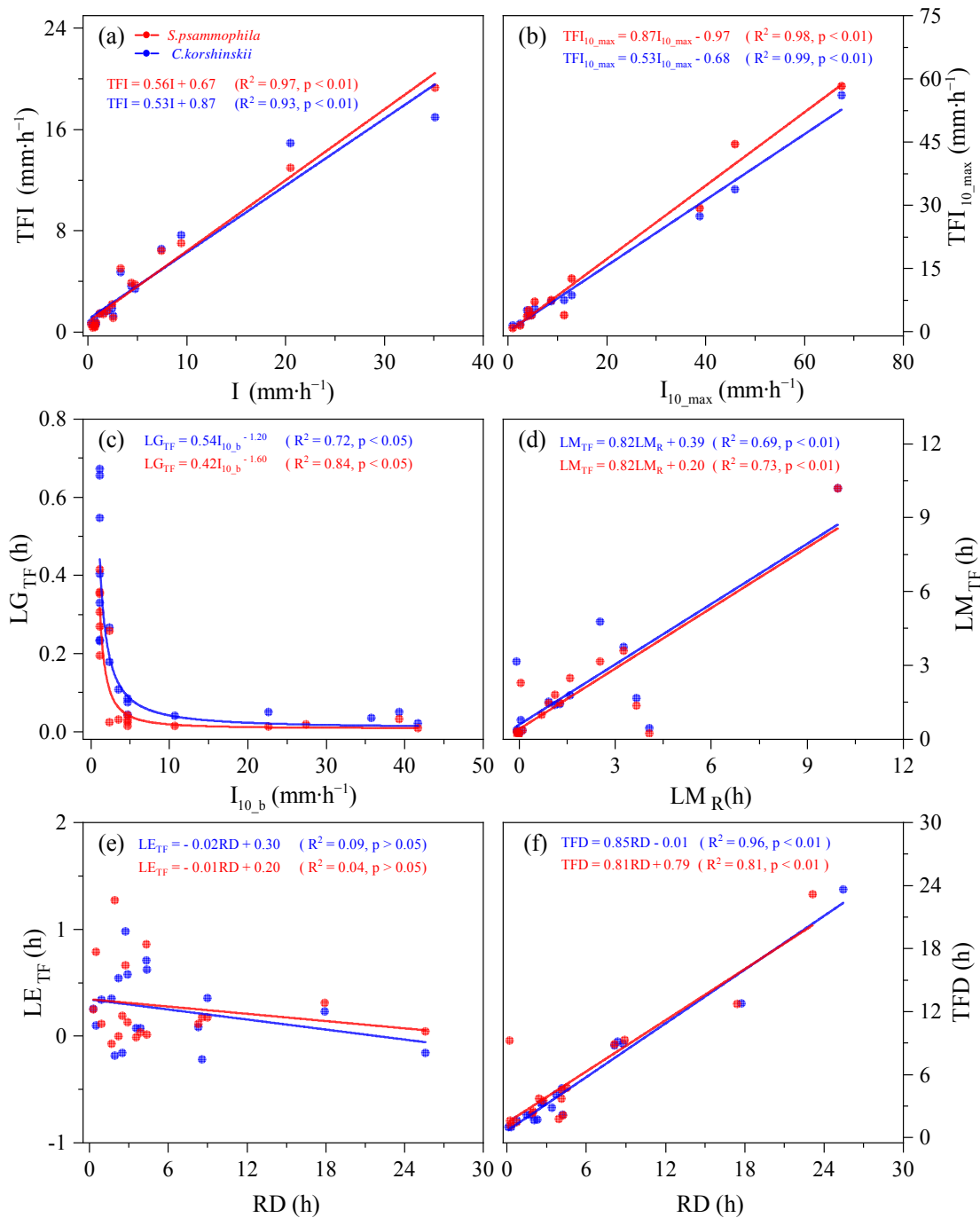
Figure 7. Relationships of intra-event throughfall variables with meteorological characteristics for *C. korshinskii* and *S. psammophila*. All the variables are explained in Table 2.

Figure 8. Relationships of intra-event stemflow variables with meteorological characteristics for *C. korshinskii* and *S. psammophila*. All the variables are explained in Table 2.